

**Spin-polarized quasiparticle control in a double spin-filter tunnel junction**

P. K. Muduli\*

*Department of Materials Science and Metallurgy, University of Cambridge, 27 Charles Babbage Road, Cambridge CB3 0FS, United Kingdom*

(Received 25 May 2017; published 24 July 2017)

Spin-polarized quasiparticles can be easily created during spin-filtering through a ferromagnetic insulator (FI) in contact with a superconductor due to pair breaking effects at the interface. A combination FI-N-FI sandwiched between two superconductors can be used to create and analyze such spin-polarized quasiparticles through their nonequilibrium accumulation in the middle metallic (N) layer. We report spin-polarized quasiparticle regulation in a double spin-filter tunnel junction in the configuration NbN-GdN1-Ti-GdN2-NbN. The middle Ti layer provides magnetic decoupling between two ferromagnetic GdN and a place for nonequilibrium quasiparticle accumulation. The two GdN(1,2) layers were deposited under different conditions to introduce coercive contrast. The quasiparticle tunneling spectra has been measured at different temperatures to understand the tunneling mechanism in these double spin-filter junctions. The conductance spectra were found to be comparable to an asymmetric SINIS-type tunnel junction. A hysteretic R-H loop with higher resistance for the antiparallel configuration compared to parallel state was observed, asserting the spin-polarized nature of quasiparticles. The hysteresis in the R-H loop was found to disappear for subgap bias current. This difference can be understood by considering modification of the interlayer coupling due to nonequilibrium spin-polarized quasiparticle accumulation in the Ti layer.

DOI: [10.1103/PhysRevB.96.024514](https://doi.org/10.1103/PhysRevB.96.024514)**I. INTRODUCTION**

In superconductors, below the critical temperature  $T_C$  the electrons with opposite momentum and spin are bound in (singlet) Cooper pairs; therefore, they can transport only charge but not spin. At finite temperature a fraction of Cooper pairs is broken into excited states called (Bogoliubov) quasiparticles which are capable of transporting both charge and spin. Quasiparticles can be created inside a superconductor while injecting current through a tunnel barrier or by irradiating electromagnetic radiation with energy,  $h\nu \gg \Delta$ , where  $\nu$  is the frequency of radiation and  $\Delta$  is the superconducting energy gap (binding energy of Cooper pairs) [1]. Eventually with time the quasiparticles recombine to form Cooper pairs after emitting a phonon maintaining equilibrium. In the presence of extra disturbances, quasiparticle concentration can be increased and driven out of equilibrium, which follows a non-Fermi Dirac distribution function. The number and dynamics of these nonequilibrium quasiparticles has been the subject of intense research lately, as they are the primary source of decoherence in almost all superconducting electronics [2]. However, these nonequilibrium quasiparticles can be very advantageous for spintronics purposes as they have a very large mean free path ( $\lambda_Q$ ) compared to ordinary electrons [3].

*Quasiparticle spintronics* is not new and has been out there since the 1970s. Meservay and Tedrow have shown that spin polarization of various ferromagnets can be determined by injecting spin-polarized quasiparticles from a ferromagnet into a superconductor [4]. Recently, quasiparticle spintronics have seen renewed interest and most of the study has been focused on spin transport inside superconductors through quasiparticle excitations [5–10]. It is now believed that spin and charge are transported by separate quasiparticle excitations in a superconductor [7,11]. Signatures of spin transport over

distances up to several micrometers has been observed in Zeeman split superconductors in proximity to a ferromagnetic insulator [12–16]. Many spintronics phenomena, like the quasiparticle-mediated spin Hall effect (SHE) [17,18], the Seebeck effect induced by spin-polarized quasiparticles [19], quasiparticle spin resonance [7,20], etc., have been experimentally observed. However, many fundamental aspects of quasiparticle spintronics remains poorly understood. The most interesting prospect of quasiparticle spintronics would be to explore the possibility to take quasiparticles out of a superconductor into a normal metal and introduce spintronics functionality. One obvious system for this type of study is a double spin-filter device of the type S-FI-N-FI-S (here FI is ferromagnetic insulator, N is normal metal, and S is the superconductor), which is analogous to conventional SINIS-type devices [5,21]. Double-barrier superconducting tunnel junctions of the S-I-N(s)-I-S structure have been extensively studied to cool down the electron in the normal metal (N) from 300 to 100 mK or to enhance superconductivity in the middle *s* layer [22–24]. Operation of these devices is based on the modification of the quasiparticle distribution function in the N region of the junction, which can have a non-Fermi Dirac form leading to a measurable outcome. Blamire *et al.* have observed enhancement in the superconductivity of Al up to 4 K in a symmetric Nb-AlO<sub>x</sub>-Al-AlO<sub>x</sub>-Nb double-barrier junction [25]. Enhancing superconductivity by means of nonequilibrium effects has received substantial theoretical interest but still remains controversial experimentally [26–28].

Spin-filter tunnel junctions comprising superconductors produce a great amount of spin-polarized quasiparticles by enforcing Cooper pairs to split while tunneling [29]. Therefore double spin-filter devices of the type S-FI-N-FI-S provide a unique opportunity to explore quasiparticle spintronics through nonequilibrium quasiparticle accumulation in the middle N layer [30,31]. In this kind of device when the two spin-filter layers are parallel to each other, no spin accumulation happens, as the number of injected spin-up electrons

\*muduli.ps@gmail.com

in the N layer is same as the number of spin-up electrons leaving it. In the antiparallel case finite nonequilibrium spin accumulation in the middle layer is expected, which relaxes through spin-flip processes. A double spin-filter device with superconductivity-induced nonequilibrium has been predicted to show huge TMR,  $\sim 10^2\%$ – $10^6\%$ , which can be tuned with biasing voltage and temperature [32,33].

In this paper, we report fabrication of double spin-filter devices in which a metallic Ti layer is symmetrically connected to two identical superconductors through ferromagnetic (GdN) tunnel barriers. We present quasiparticle tunneling spectra measurements on NbN-GdN-NbN, NbN-Ti-GdN-NbN, and NbN-GdN1-Ti-GdN2-NbN tunnel junctions measured at different temperatures. We explore the possibility of creating nonequilibrium quasiparticle accumulation in the Ti layer and its effect on the magnetic coupling between the two GdN layers. The R-H loops of the double spin-filter tunnel junctions were measured at different bias currents and temperature to explore these effects.

## II. EXPERIMENTAL

Multilayer structures NbN-GdN1-Ti-GdN2-NbN were grown by dc sputtering in an ultrahigh vacuum (UHV) chamber at room temperature. The NbN and GdN layers were deposited under similar conditions as described in Refs. [34–38]. It has been observed that the magnetic and electrical property of GdN is sensitive to deposition conditions and can be tuned by changing different Ar and N<sub>2</sub> gas mixtures and deposition powers [34]. The two GdN(1,2) layers were grown with different gas mixtures in order to introduce coercive contrast. The GdN1 and GdN2 layers were deposited with 8% and 4% Ar – N<sub>2</sub> gas mixture, respectively. The Ti layer was grown in a pure Ar gas environment with a pressure of 1.5 Pa and sputtering power of 40 W. The thickness of the top and bottom NbN layers were kept fixed at 50 nm, while the thicknesses of the GdN and Ti layers were varied in different depositions. Eight multilayer stacks with different thicknesses of Ti were grown in the same deposition in the sequence NbN-GdN1-Ti-GdN2-NbN from left to right.

The double junctions were fabricated in a mesa structure in which the junction area ( $7\ \mu\text{m} \times 7\ \mu\text{m}$ ) was defined by CF<sub>4</sub> plasma etching and Ar-ion milling. The fabrication process is similar as described in Ref. [36], except these devices were Ar-ion milled for 14 min instead of 4 min to ensure complete milling of Ti until the bottom NbN layer. Figure 2(d) shows schematic of the double tunnel junction in the mesa structure with measurement scheme. The electrical characterization of the devices up to 4.2 K were done in a custom-made dipstick. For 300-mK measurements a He-3 sorption insert from Cryogenics Ltd. was used. The differential conductance  $dI/dV$  of the junctions at 300 mK were obtained by numerically differentiating measured  $I$ – $V$  curves. Conductance spectra at 4.2 K were obtained with standard lock-in technique. The R-H loops were measured with a dc current source and nanovoltmeter. In this report we show the results of one representative double junction. Measurements done on other junctions on the same chip and devices with different thickness of Ti are shown in the Supplemental Material [39]. All the data reported in the

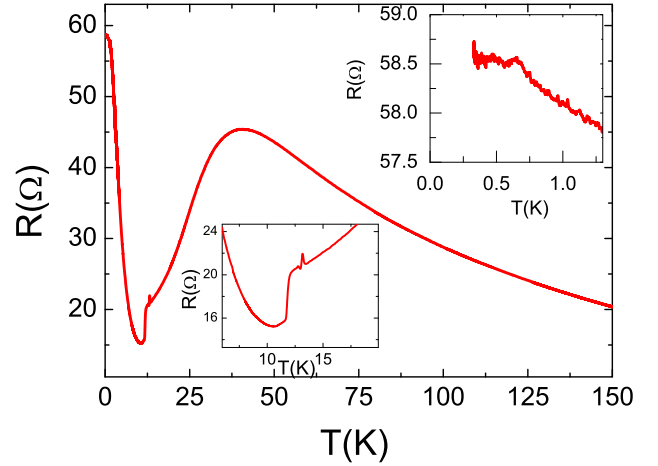


FIG. 1. Temperature dependence of resistance of the NbN(50 nm) – GdN(2 nm–8%) – Ti(8 nm) – GdN(2 nm–4%) – NbN(50 nm) double spin-filter tunnel junction. The measurement was done using a current  $I = 10\ \mu\text{A}$ . The upper inset shows  $R(T)$  in the range 0.3 to 1.3 K. Lower inset shows  $R(T)$  close to  $T_C$ .

manuscript were found to be extremely reproducible, as shown in the supplemental figures [39].

## III. RESULTS AND DISCUSSION

Figure 1 shows the temperature dependence of resistance of a double spin-filter tunnel junction with an 8-nm-thick Ti spacer. A semiconducting behavior can be seen until 35 K and metalliclike behavior below it due to onset of spin filtering at the Curie temperature,  $T_{\text{Curie}} \approx 35\ \text{K}$  of GdN layers. The  $R(T)$  is similar to a single NbN-GdN-NbN spin-filter tunnel junction [35,40]. The superconducting transition of NbN can be seen to start at  $T_C \approx 13\ \text{K}$ . The transition was found to be broad with a width of  $\sim 1.7\ \text{K}$  as shown in the lower inset

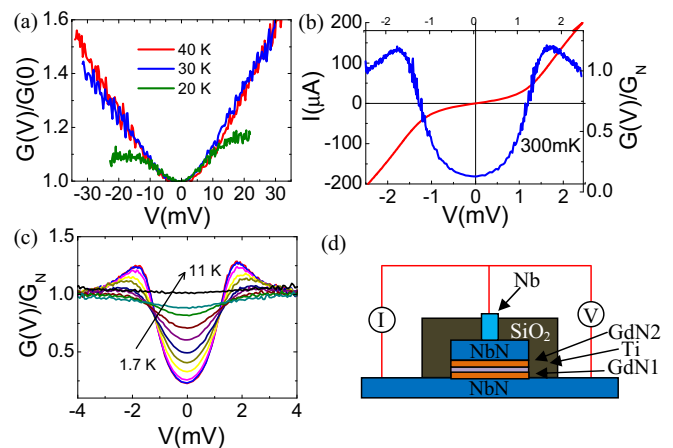


FIG. 2. (a) Normalized conductance spectra  $G(V)/G(0)$  of the double spin-filter tunnel junction measured at 40, 30, and 20 K. (b) The  $I$ – $V$  and normalized conductance spectra of the same junction measured at 300 mK. (c) Normalized conductance spectra of the junction measured in the temperature range 1.7–11 K. (d) Schematic of the double tunnel junction in the mesa structure with measurement scheme.

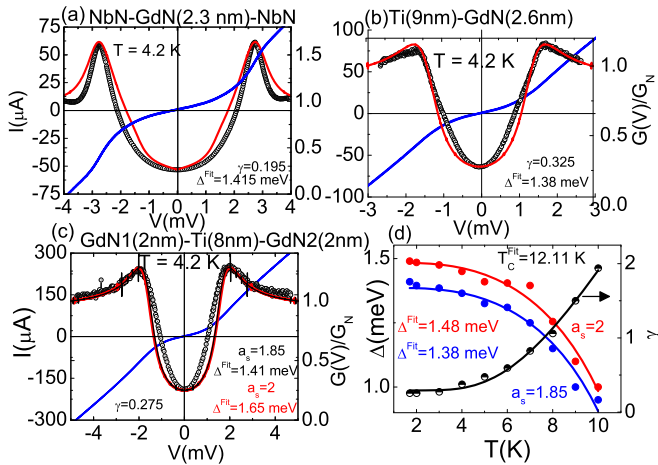


FIG. 3. (a)  $I-V$  and normalized conductance spectra  $G(V)/G_N$  of NbN-GdN(2.3 nm)-NbN tunnel junction. The red solid line represents fitting to the S-I-S tunneling model with fitting parameter  $\Delta = 1.415$  meV and  $\gamma = 0.195$ . (b)  $I-V$  and normalized conductance spectra  $G(V)/G_N$  of NbN-Ti(9 nm)-GdN(2.6 nm)-NbN tunnel junction. The red solid line represents fitting to the N-I-S tunneling model with fitting parameter  $\Delta = 1.38$  meV and  $\gamma = 0.325$ . (c)  $I-V$  and normalized conductance spectra  $G(V)/G_N$  of NbN-GdN1(2 nm)-Ti(8 nm)-GdN2(2 nm)-NbN tunnel junction. The red solid line represents fitting to the S-I-N-I-S tunneling model with asymmetry parameter  $a_s = 2$  (red) and 1.85 (black). (d) Temperature evolution of the fitting parameters  $\Delta$  and  $\gamma$  found from fitting Eq. (1) to the conductance spectra shown in Fig. 2(c). The red ( $a_s = 2$ ) and blue ( $a_s = 1.85$ ) solid lines are the fitting to the BCS-type temperature dependence,  $\Delta(T) = \Delta(0) \tanh[1.74\sqrt{(T_C - T)/T}]$  with  $T_C = 12.11$  K. Black solid line is the fitting to an exponential of the form  $\gamma \propto e^{-\zeta/T}$  [51].

of Fig. 1. This is due to the difference in  $T_C$  of the top and bottom NbN in the double tunnel junction. The  $R(T)$  of some other double tunnel junctions are shown in the Supplemental Material (SFig. 3, Ref. [39]). For measurements done with a bias voltage smaller than gap voltage, i.e.,  $eV < 2\Delta$ , the resistance was found to increase rapidly below  $T_C$  of NbN. The electrical transport below  $T_C$  is determined by quasiparticles. For bias voltage in the subgap region the tunneling current is weakly dependent on bias voltage and scales with temperature-dependent quasiparticle density  $n(T) \propto \sqrt{T} e^{-\frac{\Delta}{k_B T}}$  [41]. Therefore, the temperature dependence of subgap resistance follows an exponential dependence,  $R(T) \propto e^{-\Delta/k_B T}$ , with a constant parallel leakage resistance [42]. The upper inset in Fig. 1 shows  $R(T)$  in the range 1.3 to 0.3 K. Bulk Ti is known to be a superconductor with  $T_C \approx 0.49$  K. However, we could not observe any superconducting transition of Ti in our devices until 0.3 K. This might be due to large suppression of  $T_C$  of the thin Ti layer sandwiched between two magnetic GdN layers.

### A. Tunneling behavior

A double tunnel junction is essentially made of two tunnel junctions in series. In our NbN-GdN1-Ti-GdN2-NbN double tunnel-junction devices there are two tunnel junctions NbN-GdN1-Ti ( $J_{n1}$ ) and Ti-GdN2-NbN ( $J_{n2}$ ) in series. As the two

tunnel junctions are deposited in opposite sequence they most likely have different resistances,  $R_{Jn1}$  and  $R_{Jn2}$ . Besides, the NbN-GdN interface is expected to be more resistive than the Ti-GdN interface due to different Schottky barrier heights,  $\Phi_{Sh} = W - E_g^{\text{GdN}}$ , where  $E_g^{\text{GdN}}$  is the band gap of GdN and  $W$  is the work function of the metal. As the work function of NbN,  $\sim 4.7$  eV [43], is larger than that of Ti,  $\sim 4.3$  eV [44], the NbN-GdN interface has a lower transparency than the Ti-GdN interface. Therefore, the double tunnel-junction NbN-GdN1-Ti-GdN2-NbN is most likely to develop asymmetry even with an ideal interface without considering fabrication issues. Asymmetry can also arise due to distortion of the barrier shape from a standard rectangular potential barrier. Distortion from an ideal rectangular shape can easily occur in the GdN(1,2) tunnel barriers, as both the layers are polycrystalline and deposited with a different Ar-N<sub>2</sub> gas mixture. We also observed a small offset of parabolic conductance from  $V = 0$  usually expected for an asymmetric tunnel barrier according to the BDR (Brinkman-Rowell-Dynes) model (see SFig. 17, Ref. [39]) [45]. Traditionally a double tunnel junction with superconductors has been studied with structure Nb-Al<sub>2</sub>O<sub>3</sub>-Al-Al<sub>2</sub>O<sub>3</sub>-Nb or Nb-NbO<sub>x</sub>-Al-AlO<sub>x</sub>-Nb [46,47]. The Al spacer is most popular due to its tendency to form a high-quality pinhole-free native oxide. In this kind of tunnel junction AlO<sub>x</sub> provides a large barrier height,  $\sim 1.7$  to 2.5 eV [48], which makes it possible to create a potential well and observe fascinating effects like resonant tunneling in double-barrier tunnel junctions. But in the case of GdN the barrier height is usually small,  $\sim 10$ –100 meV [40], and therefore a more transparent tunnel barrier is expected.

The  $I-V$  and  $dI/dV - V$  measurements were done at different temperatures to understand the tunneling nature of the double junctions. Figure 2 shows the conductance spectra  $G(V)$  ( $=dI/dV$ ) normalized to its value at  $V = 0$  measured at different temperatures above the  $T_C$  of NbN. Parabolic conductance spectra suggest a tunneling-type transport in these devices. For the  $dI/dV$  measurements at 20 K deviation from parabolic behavior above  $\pm 10$  mV is probably due to exchange splitting of the GdN tunnel barrier below the  $T_{\text{Curie}}$ . Tunneling through magnon excitations can also open up additional inelastic channels leading to deviation from parabolic behavior. A small asymmetry can also be seen in the conductance spectra which suggests the two tunnel junctions involved in the double tunnel junction have different resistances,  $R_{Jn1}$  and  $R_{Jn2}$ . The conductance spectra of the same junctions were also measured below  $T_C$  of NbN. The normalized  $dI/dV$  spectra measured in the temperature range 1.7 to 11 K are shown in Fig. 2(c). The clear appearance of a superconducting gap validates a tunneling-type transport in these double tunnel junctions. Figure 2(b) shows  $I-V$  and  $dI/dV$  measurement done on the same junction at 300 mK. Two conductance peaks separated by  $4\Delta \approx 3.3$  meV can be observed. The superconducting gap  $\Delta$  of NbN is suppressed along with smearing of gap edges, probably due to magnetic GdN [49]. In SINIS tunnel junctions the nonequilibrium effects usually lead to subgap step structures whose position and amplitude strongly depend on the temperature [28,50]. In some cases a much sharper gap-edge structure is considered as an evidence of the nonequilibrium effects [47]. However, none of these features can be seen in the conductance spectra, as

shown in Figs. 2(b) and 2(c). The reason for this is discussed below.

Below the  $T_C$  of NbN the conductance spectra of our devices can be understood in terms of an asymmetric SINIS tunnel

model with an asymmetry parameter  $a_s = \frac{2x}{1+x}$  ( $1 \leq a_s \leq 2$ ) with  $x = \frac{R_{\text{int}}}{R_{\text{int}}}$ . The normalized conductance of an asymmetric SINIS tunnel junction can be written as [52]

$$\frac{G(V)}{G_N} = \frac{1}{a_s} \frac{d}{d(eV)} \int_{-\infty}^{+\infty} N_S(E) \left[ f_N \left( E - a_s \frac{eV}{2} \right) - f_N \left( E + a_s \frac{eV}{2} \right) \right] dE, \quad (1)$$

where  $f_N(E)$  is the nonequilibrium distribution function inside the Ti layer and can be expressed as

$$f_N(E) = \frac{N_S(E - a_s \frac{eV}{2}) f_0(E - a_s \frac{eV}{2}) + N_S(E - a_s \frac{eV}{2}) f_0(E - a_s \frac{eV}{2}) + \frac{f_0(E)}{\tau_E \Gamma}}{N_S(E - a_s \frac{eV}{2}) + N_S(E - a_s \frac{eV}{2}) + \frac{1}{\tau_E \Gamma}}. \quad (2)$$

Here  $f_0(E, T) = \frac{1}{1 + \exp(E/k_B T)}$  is the Fermi-Dirac function at temperature  $T$ . The superconducting quasiparticle density of state with Dynes parameter  $\gamma$  is given by  $N_S(E) = N(0) |\text{Re}(\frac{E/\Delta - i\gamma}{\sqrt{(E/\Delta - i\gamma)^2 - 1}})|$ . Here  $\gamma$  incorporates a finite lifetime of quasiparticles in the superconductor. In Eq. (2),  $\tau_E$  is the relaxation time representing the time scale for interchange of energy between the quasiparticle and the rest of the system. Here  $\Gamma$  is the tunneling injection rate and is given by  $\Gamma = \frac{2}{N_N(E_F) R_N A L e^2}$ , where  $N_N(E_F)$  is the normalized density of states of Ti,  $R_N$  is the normal state resistance of Ti, and  $A$  and  $L$  are the cross-section area and length of the normal metal (Ti), respectively. Clearly, the influence of nonequilibrium processes can be enhanced by increasing  $\Gamma$  with smaller tunnel junction volume and lower tunneling resistance.

Now we discuss conditions for nonequilibrium. The distribution function of quasiparticles inside the normal metal is mainly determined by the ratio of the rate of injection and relaxation of quasiparticles into it. Usually for  $\tau_E \Gamma \gg 1$  (injection rate exceed relaxation rate) the distribution function in the normal metal deviates from the thermal equilibrium Fermi distribution function  $f_0(E, T)$ , and if  $\tau_E \Gamma \ll 1$  (equilibrium), the normal metal follows a Fermi distribution function. The conditions  $\tau_E \Gamma \rightarrow 0$  and  $\tau_E \Gamma \rightarrow \infty$  correspond to complete equilibrium and nonequilibrium, respectively. In a low-resistance GdN tunnel the barrier  $\Gamma$  is increased but energy relaxation time  $\tau_E$  is decreased. The energy relaxation rate is determined by electron-electron interactions, electron-phonon interactions, and magnetic sources of relaxation. In a double spin-filter tunnel junction with spin-polarized quasiparticles the energy relaxation time can be written as

$$\frac{1}{\tau_E} = \frac{1}{\tau_{e-e}} + \frac{1}{\tau_{e-ph}} + \frac{1}{\tau_{sf}}, \quad (3)$$

where  $\tau_{e-e}$  is electron-electron scattering time,  $\tau_{e-ph}$  is electron-phonon scattering time, and  $\tau_{sf}$  is spin-flip scattering time. Spin-flip scattering caused by spin-orbit interactions and static magnetic impurities are elastic and may not cause energy relaxation directly. However, spin-flip scattering caused by electron-magnon scattering is inelastic and can relax energy [53–56]. Clearly in the case of a double spin-filter tunnel

junction,  $\tau_E$  is smaller compared to a nonmagnetic SINIS tunnel junction due to an additional last term in Eq. (3). As  $\tau_E < (\tau_{e-e}, \tau_{e-ph}, \tau_{sf})$ , the energy relaxation time is limited by the shortest time scale, i.e.,  $\tau_{sf}$ . Therefore, driving the middle Ti layer far from equilibrium in the double spin-filter tunnel junction is not trivial like a SINIS tunnel junction with nonmagnetic elements. Our double spin-filter tunnel junctions can be reasonably assumed as a series connection of SIN and NIS junctions where the energy distribution function in the interlayer is the equilibrium Fermi distribution function, i.e.,  $f_N(E, T) \approx f_0(E, T)$ .

Figures 3(a)–3(c) show  $I$ - $V$  and conductance spectra of different types of tunnel junctions measured at 4.2 K in the same experimental setup (measured with lock-in technique). In a typical NbN-GdN-NbN tunnel junction the conductance spectra show a superconducting gap  $\Delta(4.2 \text{ K}) \approx 1.4$ – $1.5$  meV depending on the tunnel barrier thickness and transparency. See the Supplemental Material (SFig. 13, Ref. [39]) for the conductance spectra of NbN-GdN-NbN tunnel junctions with different thickness of GdN. Figure 3(a) shows the conductance spectra of a NbN-GdN (2.3 nm)–NbN tunnel junction measured at 4.2 K. The red solid line is the fit to the typical SIS tunneling model with fitting parameter  $\Delta = 1.415$  meV and  $\gamma = 0.195$ . (See Supplemental Material for SIS tunnel model used for fitting [39].) Figure 3(b) shows the conductance spectra of a NbN-Ti(9 nm)–GdN(2.6 nm)–NbN tunnel junction. As the thickness of the Ti ( $\sim 9$  nm) in this type of device is larger than both the superconducting coherence length  $\xi_{\text{NbN}} \approx 4.1$  nm [38] and  $\xi_{\text{Ti}}^N \approx 3.6$  nm [57] ( $\xi_{\text{Ti}}^N$ , normal state coherence length of Ti), this type of tunnel junction can be considered as an NIS-type tunnel junction. The red solid line shows fitting of the NIS tunnel model to the conductance spectra with fitting parameter  $\Delta = 1.38$  meV and  $\gamma = 0.325$ . (See Supplemental Material [39] for more detailed study of NIS-type tunnel junctions [49].) Figure 3(c) shows conductance spectra of the double tunnel junction NbN-GdN1(2 nm)–Ti(8 nm)–GdN2(2 nm)–NbN. The conductance spectra looks more like a NIS-type tunnel junction. The red and black solid lines show fitting to Eq. (1) with asymmetry parameters  $a_s = 2$  and  $a_s = 1.85$ , respectively. Note that the asymmetry parameter is limited to have values in the range  $1 \leq a_s \leq 2$ . For  $a_s = 1$ , Eq. (1) corresponds to a symmetric

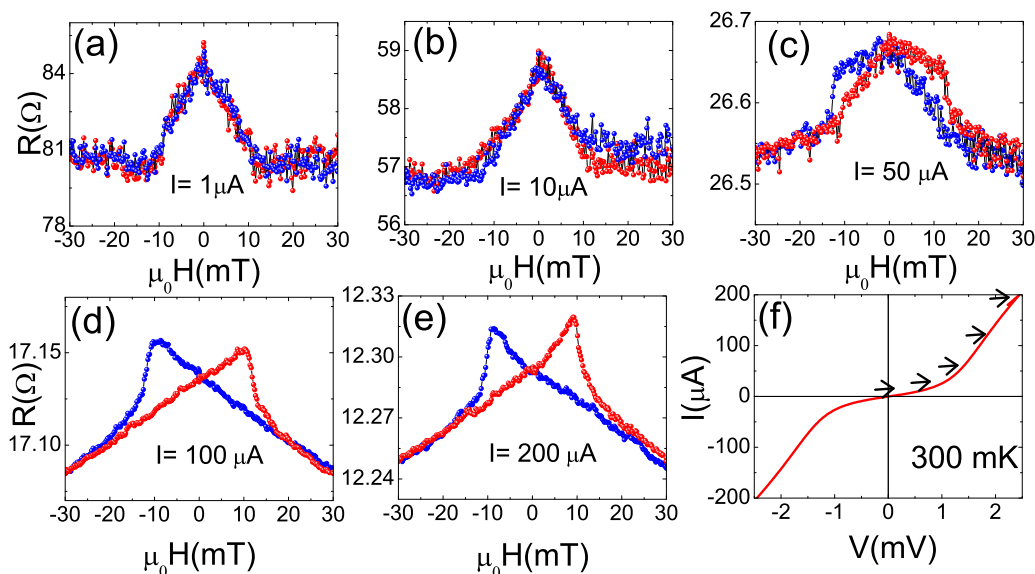


FIG. 4. R-H loops measured with different bias current: (a)  $1 \mu\text{A}$ , (b)  $10 \mu\text{A}$ , (c)  $50 \mu\text{A}$ , (d)  $100 \mu\text{A}$ , and (e)  $200 \mu\text{A}$ . (f) The  $I-V$  curve of the junction at the same temperature ( $T = 300 \text{ mK}$ ). The arrows indicate different points in the  $I-V$  curve where the R-H loop was measured. Gradual disappearance of the hysteresis in the R-H loop can be seen as bias current is reduced to below subgap value.

SINIS tunnel junction, while for  $a_s = 2$  it reduces to a single SIN tunnel junction. Fitting Eq. (1) with the asymmetry parameter  $a_s = 2$  to the conductance spectra shown in Fig. 3(c) gives  $\Delta = 1.65 \text{ meV}$ . This is much larger than the value of  $\Delta$  found from the SIS- and NIS-type tunnel junction as shown in Figs. 3(a) and 3(b). Therefore our double tunnel junction is not a single NIS type and most likely a SINIS-type double tunnel junction with a large asymmetry. The black solid line shows fitting to Eq. (1) with  $a_s = 1.85$ . This gives  $\Delta = 1.41 \text{ meV}$ , which is more reasonable. Note that  $a_s = 1.85$  means the resistance ratio between the two tunnel junctions:  $R_{Jn1}/R_{Jn2} \approx 12.3$ . This can easily happen considering different deposition conditions. Figure 3(d) shows the temperature dependence of  $\Delta$  and  $\gamma$  obtained from fitting conductance spectra measured at different temperatures shown in Fig. 2(c). The conductance spectra was fitted for two asymmetry parameters  $a_s = 1.85$  (blue) and  $a_s = 2$  (red) with the same smearing parameter  $\gamma$ . The red and blue solid lines show fitting to BCS-type temperature dependence:  $\Delta(T) = \Delta(0) \tanh(1.74\sqrt{(T_C - T)/T})$ . For both the asymmetry parameter  $T_C = 12.11 \text{ K}$  was found. The smearing parameter  $\gamma$  was found to decrease rapidly with temperature. The black solid line shows fitting to an exponential decay,  $\gamma \propto e^{-\zeta/T}$ , where  $\zeta$  is the decay constant.

### B. Spin-valve behavior

In a SINIS-type tunnel junction when the bias voltage  $eV$  exceeds  $2\Delta$ , quasiparticle current is produced from the energy gained primarily from the applied bias voltage. Besides, even for voltages less than  $2\Delta$  at a finite temperature thermally excited quasiparticles above the gap are present whose number exponentially reduce as temperature is lowered below  $T \ll T_C$ . However, in a double spin-filter tunnel junction, additional spin-polarized quasiparticles are present due to pair breaking processes which equally populate the electron and hole-like excitation spectrum [29]. In a double spin-filter tunnel junction

the spin-polarized quasiparticle current can be turned ON and OFF by reorienting the magnetization of the two spin-filter barriers parallel and antiparallel with respect to each other, respectively.

The presence of the superconducting gap in the conductance spectra induces an energy selectivity of quasiparticle tunneling. Therefore, in double spin-filter devices the number and the energy of the quasiparticles can be drastically altered if a bias voltage above and below the gap is applied. The R-H loops measured above and below the gap voltage can provide valuable information about nonequilibrium quasiparticle accumulation in the middle metallic (Ti) layer [58]. Figures 4(a)–4(e) show R-H loops of the double spin-filter tunnel junction measured at  $300 \text{ mK}$  with different bias currents. The  $I-V$  curve measured at the same temperature is shown in Fig. 4(f). The conductance spectra gap edges can be seen at  $\sim 1.68 \text{ meV}$ , which corresponds to a bias current of  $I = 99 \mu\text{A}$ . At bias current  $I = 200 \mu\text{A}$  a clear hysteretic R-H loop with resistance peaks near  $\pm 10 \text{ mT}$  can be observed. As the coercive field of a single GdN layer is typically  $\sim 5 \text{ mT}$  [35,59], the hysteretic R-H loop observed in these double tunnel junctions is due to relative magnetization orientation of the two GdN(1,2) layers. A broad switching is observed in this case due to the multidomain nature of the GdN layers. One striking thing to note is that the hysteresis in the R-H loops was found to disappear as the current was decreased from  $200$  to  $1 \mu\text{A}$ . However, an overall high resistance state can still be seen in the magnetic field range  $\pm 15 \text{ mT}$  when the two magnetic GdN(1,2) layers are not parallel to each other. The number of charge carriers (quasiparticles) that can transport charge through the S-FI-N-FI-S structure is reduced drastically as the bias voltage is reduced below the gap voltage. This can be seen as an increase in the resistance of the double spin-filter tunnel junction from  $12$  to  $81 \Omega$  as the bias current is reduced from  $200$  to  $1 \mu\text{A}$ . The R-H loops were also measured at different temperatures, and similar behavior was found at

all temperatures below  $T_C$  of NbN. The hysteresis in the R-H loop was found to disappear above 15 K (see supplementary figure SFig. 4, Ref. [39]). Although,  $T_{\text{Curie}}$  of GdN  $\approx$  35 K, the absence of a hysteretic R-H loop above 15 K suggests the absence of a well-established parallel and antiparallel state. A linear decrease in resistance with magnetic field can still be observed above 15 K, confirming the magnetic nature of individual GdN layers above 15 K.

The switching behavior can be understood by considering spin-polarized quasiparticle accumulation and relaxation inside the Ti layer. A finite spin-polarized quasiparticle accumulation is expected inside the Ti layer when the two GdN(1,2) layers are antiparallel to each other. Therefore conductance is reduced and the resistance for the antiparallel state is expected to be higher than that for the parallel configuration. Also, spin-polarized quasiparticle accumulation can modify the interlayer exchange coupling. The absence of a hysteretic R-H loop at subgap bias current is most likely due to the suppression of interlayer exchange coupling between two GdN(1,2) layers. This is expected, as magnetic coupling is usually suppressed in the F-S-F trilayer system below the critical temperature  $T_C$  of the superconductor [60,61]. Suppressed magnetic coupling has been observed in Fe<sub>4</sub>N-NbN-Fe<sub>4</sub>N [62], (100)-oriented GdN/W/NbN/W multilayers [63] and GdN-NbN-GdN trilayers [64]. Recently, a different kind of interlayer exchange coupling mechanism in GdN-Nb-GdN has been proposed [59]. Interlayer exchange coupling between ferromagnetic metallic layers separated by a superconducting spacer has been investigated extensively in many systems and a detailed discussion is beyond the scope of this paper [60,61,65–68]. A more detailed experimental study with different thickness of the normal-metal spacer is needed to understand the interlayer exchange mechanism in

the presence of nonequilibrium quasiparticles in these double spin-filter tunnel junctions.

#### IV. CONCLUSIONS

In conclusion, we have fabricated a double spin-filter tunnel junction in the configuration NbN-GdN1-Ti-GdN2-NbN. The conductance spectra in these double spin-filter tunnel junctions were found to be analogous to a highly asymmetric SINIS-type tunnel junction. We have demonstrated spin-polarized quasiparticle control in these double spin-filter tunnel junctions with R-H measurements done at different bias voltages above and below the gap voltage  $eV = 2\Delta$ . Hysteresis in the R-H loop was found to be absent for subgap bias currents. The absence of hysteresis in the R-H loop may be considered as an experimental signature of nonequilibrium spin-polarized quasiparticle accumulation. Although nonequilibrium effects cannot be inferred conclusively from these experiments, these preliminary experimental results are of fundamental importance and call for further experimental and theoretical investigation. Magnetic manipulation of quasiparticles is pivotal for the advancement of quasiparticle spintronics [69].

#### ACKNOWLEDGMENTS

The idea of a double spin-filter tunnel junction based on GdN is a part of the proposal ERC (European Research Council, Belgium) Advanced Grant (2011) ‘SUPERSPIN’; Principal Investigator: Prof M. G. Blamire. The experimental data presented in this manuscript was collected by P.K.M. during June 2012 to April 2015. P.K.M. acknowledges Dr. David Gustafsson for assistance during the 300-mK measurement.

- 
- [1] E. G. Wolf, *Principles of Electron Tunneling Spectroscopy* (Oxford University Press, Oxford, 1985).
  - [2] John M. Martinis, M. Ansmann, and J. Aumentado, *Phys. Rev. Lett.* **103**, 097002 (2009).
  - [3] K. Yu. Arutyunov, H.-P. Auraneva, and A. S. Vasenko, *Phys. Rev. B* **83**, 104509 (2011).
  - [4] P. M. Tedrow and R. Meservey, *Phys. Rev. B* **7**, 318 (1973); R. Meservey, D. Paraskevopoulos, and P. M. Tedrow, *Phys. Rev. Lett.* **37**, 858 (1976).
  - [5] H. Yang, S.-H. Yang, S. Takahashi, S. Maekawa, and S. S. P. Parkin, *Nat. Mater.* **9**, 586 (2010).
  - [6] F. Hübler, M. J. Wolf, D. Beckmann, and H. v. Löhneysen, *Phys. Rev. Lett.* **109**, 207001 (2012).
  - [7] C. H. L. Quay, M. Weideneder, Y. Chiffaudel, C. Strunk, and M. Aprili, *Nat. Commun.* **6**, 8660 (2015); C. H. L. Quay, D. Chevallier, C. Bena, and M. Aprili, *Nat. Phys.* **9**, 84 (2013).
  - [8] D. Chevallier, M. Trif, C. Dutreix, M. Guigou, C. H. L. Quay, M. Aprili, and C. Bena, *arXiv:1408.1833v2*.
  - [9] N. Poli, J. P. Morten, M. Urech, Arne Brataas, D. B. Haviland, and V. Korenivski, *Phys. Rev. Lett.* **100**, 136601 (2008).
  - [10] T. Wakamura, N. Hasegawa, K. Ohnishi, Y. Niimi, and Y. C. Otani, *Phys. Rev. Lett.* **112**, 036602 (2014).
  - [11] S. A. Kivelson and D. S. Rokhsar, *Phys. Rev. B* **41**, 11693 (1990).
  - [12] M. J. Wolf, F. Hübler, S. v. Kolenda, H. Loehneysen, and D. Beckmann, *Phys. Rev. B* **87**, 024517 (2013).
  - [13] N. Mason and M. Stehno, *Nat. Phys.* **9**, 67 (2013).
  - [14] I. V. Bobkova and A. M. Bobkov, *Phys. Rev. B* **93**, 024513 (2016).
  - [15] T. Krishtop, M. Houzet, and J. S. Meyer, *Phys. Rev. B* **91**, 121407(R) (2015).
  - [16] P. Virtanen, T. T. Heikkilä, and F. S. Bergeret, *Phys. Rev. B* **93**, 014512 (2016).
  - [17] T. Wakamura, H. Akaike, Y. Omori, Y. Niimi, S. Takahashi, A. Fujimaki, S. Maekawa, and Y. Otani, *Nat. Mater.* **14**, 675 (2015).
  - [18] S. Takahashi and S. Maekawa, *Jpn. J. Appl. Phys.* **51**, 010110 (2012).
  - [19] S. Kolenda, M. J. Wolf, and D. Beckmann, *Phys. Rev. Lett.* **116**, 097001 (2016).
  - [20] C. H. L. Quay, C. Dutreix, D. Chevallier, C. Bena, and M. Aprili, *Phys. Rev. B* **93**, 220501(R) (2016).
  - [21] G. X. Miao, J. Chang, B. A. Assaf, D. Heiman, and J. S. Moodera, *Nat. Commun.* **5**, 3682 (2014).
  - [22] M. M. Leivo, J. P. Pekola, and D. V. Averin, *Appl. Phys. Lett.* **68**, 1996 (1996).
  - [23] S. Chaudhuri and I. J. Maasilta, *Appl. Phys. Lett.* **104**, 122601 (2014).

- [24] J. P. Pekola, T. T. Heikkilä, A. M. Savin, J. T. Flyktman, F. Giazotto, and F. W. J. Hekking, *Phys. Rev. Lett.* **92**, 056804 (2004).
- [25] M. G. Blamire, E. C. G. Kirk, J. E. Evetts, and T. M. Klapwijk, *Phys. Rev. Lett.* **66**, 220 (1991).
- [26] D. R. Heslinga and T. M. Klapwijk, *Phys. Rev. B* **47**, 5157 (1993).
- [27] I. P. Nevirkovets, O. Chernyashevskyy, and J. B. Ketterson, *Phys. Rev. B* **73**, 224521 (2006).
- [28] T. M. Klapwijk, *Phys. B (Amsterdam, Neth.)* **197**, 481 (1994).
- [29] T. Tokuyasu, J. A. Sauls, and D. Rainer, *Phys. Rev. B* **38**, 8823 (1988).
- [30] Guo-Xing Miao and J. S. Moodera, *Appl. Phys. Lett.* **94**, 182504 (2009); *J. Appl. Phys.* **108**, 083910 (2010).
- [31] S. Kawabata, A. Ozaeta, A. S. Vasenko Frank, W. J. Hekking, and F. Sebastián Bergeret, *Appl. Phys. Lett.* **103**, 032602 (2013).
- [32] F. Giazotto, *Appl. Phys. Lett.* **95**, 042503 (2009).
- [33] D. C. Worledge and T. G. Geballe, *J. Appl. Phys.* **88**, 5277 (2000).
- [34] K. Senapati, T. Fix, M. E. Vickers, M. G. Blamire, and Z. H. Barber, *Phys. Rev. B* **83**, 014403 (2011).
- [35] K. Senapati, M. G. Blamire, and Z. H. Barber, *Nat. Mater.* **10**, 849 (2011).
- [36] P. K. Muduli, A. Pal, and M. G. Blamire, *Phys. Rev. B* **89**, 094414 (2014).
- [37] P. K. Muduli, X. L. Wang, J. H. Zhao, and M. G. Blamire, [arXiv:1410.6741](https://arxiv.org/abs/1410.6741).
- [38] P. K. Muduli, [arXiv:1608.08820](https://arxiv.org/abs/1608.08820).
- [39] See Supplemental Material at <http://link.aps.org/supplemental/10.1103/PhysRevB.96.024514> for tunneling spectra of NbN-GdN1-Ti(t)-GdN2-NbN tunnel junctions,  $R(T)$  of NbN-GdN1-Ti(t)-GdN2-NbN tunnel junctions, R-H loops of NbN-GdN1-Ti(8 nm)-GdN2-NbN tunnel junction measured at 2, 5, 10 and 15 K, reproducibility of spin-valve behaviour in NbN-GdN1-Ti(t)-GdN2-NbN tunnel junctions, tunneling spectra of NbN-GdN(t)-NbN tunnel junctions, tunneling spectra of NbN-GdN(t)-NbN tunnel junctions, and normalized conductance spectra near  $V = 0$  measured at 40, 30 and 20 K.
- [40] A. Pal, K. Senapati, Z. H. Barber, and M. G. Blamire, *Adv. Mater.* **25**, 5581 (2013).
- [41] J. T. Muhonen, *Rep. Prog. Phys.* **75**, 046501 (2012).
- [42] M. G. Blamire, A. Pal, Z. H. Barber, and K. Senapati, *Proc. SPIE* **8461**, 84610J (2012).
- [43] Y. Gotoh, H. Tsuji, and J. Ishikawa, *J. Vac. Sci. Technol., B: Microelectron. Process. Phenom.* **21**, 1607 (2003).
- [44] *CRC Handbook of Chemistry and Physics*, 84th ed. 2003–2004, edited by David R. Lide (CRC Press, Boca Raton, FL, 2003), pp. 12–130.
- [45] W. F. Brinkman, R. C. Dynes, and J. M. Rowell, *J. Appl. Phys.* **41**, 1915 (1970).
- [46] D. Cassel, G. Pickartz, M. Siegel, E. Goldobin, H. H. Kohlstedt, A. Brinkman, A. A. Golubov, M. Yu. Kupriyanov, and H. Rogalla, *Phys. C (Amsterdam, Neth.)* **350**, 276 (2001).
- [47] M. G. Blamie, *Supercond. Sci. Technol.* **4**, 430 (1991).
- [48] E. Cimpoiu, S. K. Tolpygo, X. Liu, N. Simonian, J. E. Lukens, K. K. Likharev, R. F. Klie, and Y. Zhu, *J. Appl. Phys.* **96**, 1088 (2004).
- [49] I. Giaever and K. Megerle, *Phys. Rev.* **122**, 1101 (1961).
- [50] Š. Gaži, V. Štrbik, and Š. Beňačka, *J. Low Temp. Phys.* **106**, 387 (1997).
- [51] All the conductance spectra shown in Fig. 2 are obtained by numerically differentiating measured  $I-V$  curves in a closed-cycle refrigerator. The conductance spectra shown in Figs. 3(a)–3(c) are obtained directly by lock-in technique in a custom-made dipstick. We have found that the conductance spectra measured in the closed-cycle refrigerator showed a slightly reduced gap compared to the measurements done in the dipstick as the junction gets coupled to different electromagnetic environments.
- [52] H. Courtois, S. Rajauria, P. Gandit, F. W. J. Hekking, and B. Pannetier, *J. Low Temp. Phys.* **153**, 325 (2008).
- [53] Y. Tserkovnyak and A. Brataas, *Phys. Rev. B* **65**, 094517 (2002).
- [54] A. Brinkman, A. A. Golubov, H. Rogalla, F. K. Wilhelm, and M. Yu. Kupriyanov, *Phys. Rev. B* **68**, 224513 (2003).
- [55] T. R. Lemberger and J. Clarke, *Phys. Rev. B* **23**, 1088 (1981).
- [56] A. Anthore, F. Pierre, H. Pothier, and D. Esteve, *Phys. Rev. Lett.* **90**, 076806 (2003).
- [57] L. Fritzsche, M. Schubert, G. Wende, and H.-G. Meyer, *Appl. Phys. Lett.* **73**, 1583 (1998).
- [58] P. S. Luo, T. Crozes, B. Gilles, S. Rajauria, B. Pannetier, and H. Courtois, *Phys. Rev. B* **79**, 140508(R) (2009).
- [59] Yi. Zhu, A. Pal, M. G. Blamire, and Z. H. Barber, *Nat. Mater.* **16**, 195 (2017).
- [60] O. Siper and B. L. Gyorffy, *J. Phys.: Condens. Matter* **7**, 5239 (1995).
- [61] C. A. R. Sa de Melo, *Phys. Rev. B* **62**, 12303 (2000); *Phys. Rev. Lett.* **79**, 1933 (1997).
- [62] J. E. Mattson, C. D. Potter, M. J. Conover, C. H. Sowers, and S. D. Bader, *Phys. Rev. B* **55**, 70 (1997).
- [63] R. M. Osgood, J. E. Pearson, C. H. Sowers, and S. D. Bader, *J. Appl. Phys.* **84**, 940 (1998).
- [64] K. Senapati, M. G. Blamire, and Z. H. Barber, *Appl. Phys. Lett.* **103**, 132406 (2013).
- [65] R. Porwal, A. Gupta, and R. C. Budhani, *J. Phys.: Condens. Matter* **28**, 506003 (2016).
- [66] K. Halterman and O. T. Valls, *Phys. Rev. B* **72**, 060514(R) (2005).
- [67] I. C. Moraru, W. P. Pratt, Jr., and N. O. Birge, *Phys. Rev. B* **74**, 220507(R) (2006).
- [68] A. Yu. Rusanov, S. Habraken, and J. Aarts, *Phys. Rev. B* **73**, 060505(R) (2006).
- [69] J. Linder and J. W. A. Robinson, *Nat. Phys.* **11**, 307 (2015).